Available online at www.sciencedirect.com

ScienceDirect

journal homepage: www.elsevier.com/locate/jtte

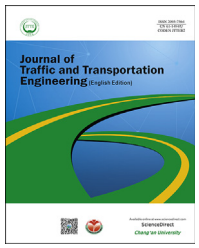

Original Research Paper

Design and field tests of a deck-extension bridge with small box girder

Junqing Xue[*], *Bruno Briseghella, Jianhui Lin, Fuyun Huang, Baochun Chen*

College of Civil Engineering, Fuzhou University, Fuzhou 350108, China

HIGHLIGHTS

- The design, construction and field tests of one deck-extension bridge with a small box girder are introduced.
- The effective bridge temperature to predict the longitudinal thermal movement of the deck-extension bridges was proposed.
- The finite element model was built by using the MIDAS program, of which the accuracy was verified by the test results.
- The longitudinal thermal movement of the deck-extension bridges under historically extreme temperatures was predicted.

ARTICLE INFO

Article history:
Received 21 April 2018
Received in revised form
27 July 2018
Accepted 29 July 2018
Available online 8 October 2018

Keywords:
Jointless bridge
Deck-extension bridge
Small box girder
Longitudinal thermal movement
Temperature distribution
Average temperature

ABSTRACT

A jointless bridge could fundamentally eliminate vulnerable deck joints, thereby meeting the need for sustainable development of bridges, especially for an expressway with high-speed traffic. In this paper, one jointless bridge (deck-extension bridge) with a small box girder in an expressway was chosen as a case study to examine the structural design, construction and field test. The field tests of the bridge indicated that the designed and constructed structures can satisfy the requirement for service performance of the deck-extension bridge. Some key technologies, such as the position of longitudinal reinforcements in the superstructure-approach slab connections and the arrangement of the sliding material layers, were introduced. The longitudinal thermal movement of the superstructure in the deck-extension bridge with a small box girder could be predicted accurately by using the average temperature of the cross section of a small box girder. The finite element model, built by using the MIDAS program, was used to analyze the temperature distribution on the cross section of a small box girder, the accuracy of which could be verified by comparing with the measured values. The maximum longitudinal thermal movement of the superstructure in deck-extension bridges with a small box girder under historically extreme temperature conditions was predicted.

* *Corresponding author*. Tel.: +86 13850152456; fax: +86 591 22865378.
E-mail addresses: junqing.xue@fzu.edu.cn (J. Xue), bruno@fzu.edu.cn (B. Briseghella), jianhui.lin@foxmail.com (J. Lin), huangfuyun@fzu.edu.cn (F. Huang), baochunchen@fzu.edu.cn (B. Chen).

Peer review under responsibility of Periodical Offices of Chang'an University.
https://doi.org/10.1016/j.jtte.2018.10.004

1. Introduction

The total length of the expressway in China exceeded 130 thousand meters at the end of 2016. Moreover, according to the Ministry of Transport of the People's Republic of China, at the end of 2016, there were 805.3 thousand bridges, of which 88.8% are bridges with short and medium spans (approximately 714.9 thousand bridges) (Ministry of Transport of the People's Republic of China, 2017). The deck joints are usually installed in the jointed bridges to absorb the longitudinal movement of the superstructure due to temperature variation and the creep and shrinkage of concrete and provide an even pavement for high-speed traffic. According to many statistical investigations of the defects in existing jointed bridges, the deck joints can be considered the most vulnerable member (Briseghella and Zordan, 2007; Xue, 2013). The deck joints can easily be damaged by the overloaded vehicles. Conversely, the damaged deck joints can be considered a very dangerous road hazard when the deck joints separate from their concrete embedment and become devices protruding out of decks towards high-speed traffic. Once refurbishment starts, the traffic must be interrupted or restricted, which is cost- or time-prohibitive (Briseghella and Zordan, 2015; Chen et al., 2014; Xue et al., 2014; Zordan and Briseghella, 2007). The concept of the continuous beam bridge can be used to eliminate the deck joints in the superstructure-pier connections in multi-span bridges (Dong et al., 2015; Zordan et al., 2011a,b). The continuous beam bridges with a small box girder are frequently used when the span length is between 20 and 35 m. Therefore, the key problem of the jointless design based on the continuous beam bridge is the elimination of the deck joints in the superstructure-abutment connections. Three types of jointless bridges can be defined based on the types of jointless abutments: the integral abutment bridge, the semi-integral abutment bridge and the deck-extension bridge (Aktan et al., 2008; Editorial Department of China Journal of Highway and Transport, 2014; Lan et al., 2017; Xue et al., 2016). The deck-extension bridge is the jointless bridge with a deck-extension abutment (Fuzhou University and Fujian Provinces No. 1 Highway Engineering Company, 2017). The movable joint is set between the superstructure and the abutment. However, the deck joints in the superstructure-abutment connections are eliminated by combining the superstructure and approach slab, as illustrated in Fig. 1. The longitudinal thermal movement of the superstructure in deck-extension bridges can be transferred to the joints between the ends of the approach slabs and the connecting roads (Aktan et al., 2008; Chen et al., 2014).

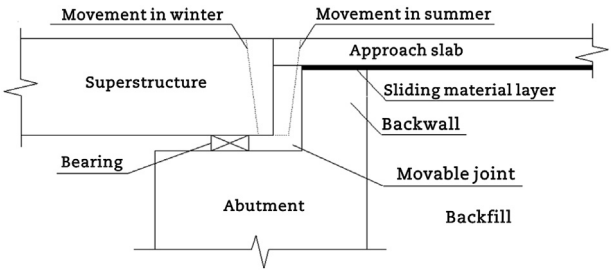

Fig. 1 – Schematic diagram of deck-extension abutment.

The deck-extension bridges were used extensively in the USA, especially when neither the integral nor the semi-integral option met the conditions of the particular structure and for retrofitting existing structures (Weakley, 2005). Approximately 3900 deck-extension bridges were constructed until the end of 2004 (Maruri and Petro, 2005). Based on the investigations of the defects in existing deck-extension bridges, the influence of different parameters on the mechanical performance of deck-extension abutments were analyzed, and the standard drawings of deck-extension abutments for Michigan Department of Transportation in the USA were proposed (Aktan et al., 2008). The standard drawings of deck-extension abutments were also proposed by some researchers for New York State Department of Transportation and Virginia Department of Transportation in the USA, as well as the Ontario Ministry of Transportation in Canada (Alampalli and Yannotti, 1998; Husain, 2004; Weakley, 2005). There were 40 jointless bridges (constructed and under construction) in China until April 2016, of which 57.5% are deck-extension bridges. However, there are only three deck-extension bridges with small box girders. There are no standard drawings of deck-extension abutments in China.

The first step of designing a jointless bridge is to ascertain the longitudinal thermal movement of the superstructure (Munoz et al., 2016; Oesterle et al., 1999). Eq. (1) is used by engineers to calculate the longitudinal thermal movement (Δl) of beams.

$$\Delta l = \alpha_c l_t \Delta t \tag{1}$$

where α_c is the thermal expansion coefficient of the material, l_t is the temperature calculation length, and Δt is the effective temperature variation.

However, the measured longitudinal thermal movements of the superstructure in jointless bridges are usually less than the corresponding calculated values determined by using Eq. (1). The measured longitudinal thermal movements of the superstructure in some jointless bridges in Michigan and Oklahoma were less than the expected values, possibly because the method used to calculate thermal movement is overly conservative and may not accurately reflect field performance (Kunin and Alampalli, 2000). The effective bridge temperature, which is referred to as the mean or average bridge temperature, was suggested to calculate the longitudinal thermal movement of the superstructure in jointless bridges. Moreover, the effective bridge temperature is influenced by many factors such as shade temperature, solar radiation, wind speed, material properties, surface characteristics, and section geometry (Aktan et al., 2008). The equations based on the minimum and maximum shade temperatures and direct solar radiation corresponding to different girder types and bridge locations were proposed to predict the minimum and maximum effective bridge temperatures in the USA (Oesterle et al., 1999). The 7-year field monitoring of four integral abutment bridges was carried out to determine that the 7-day mean temperature

(close to concrete temperature) range (−11.7 °C to 5.6 °C) is smaller than the ambient temperature range (−22.1 °C to 15.1 °C) and the design temperature range in AASHTO LRFD Bridge Design Specifications (−24.4 °C to 5.6 °C) (AASHTO, 2010; Kim and Laman, 2012). Moreover, the finite element model by using the 7-day mean temperature as the basic value for the applied numerical temperature load can predict the measured abutment movement well (Kim and Laman, 2010). The monitoring of several deck-extension bridges in China shows that the measured longitudinal movements of the superstructure in deck-extension bridges were less than the calculated values based on the characteristic values of effective temperature proposed by the code JTG D60-2015 (CCCC Highway Consultants Co., Ltd., 2015; Jin and Shao, 2009; Shao, 2014). However, there has been no unified standard for calculation of the longitudinal thermal movement of the superstructure in deck-extension bridges until the present. Determination of the longitudinal thermal movement of the superstructure in deck-extension bridges is influenced by choosing the appropriate effective bridge temperature.

In this paper, one deck-extension bridge with a small box girder in the expressway was chosen as a case study to introduce the details of design, construction and field tests. The longitudinal thermal movements of the superstructure and the temperature distribution on the cross section of the small box girder in the deck-extension bridge were measured. By comparing the calculated longitudinal movement of the superstructure in deck-extension bridges with the measured values, the method that can select the appropriate effective bridge temperature to predict the longitudinal thermal movement of the superstructure in deck-extension bridges was proposed. The finite element model was built by using the MIDAS program, of which the accuracy was verified by the test results. The longitudinal thermal movement of the superstructure in deck-extension bridges with a small box girder under historically extreme temperature conditions was predicted.

2. Jointless design

The Nansanlu Bridge is a deck-extension bridge located in Hebei Province as one part of the Beijing–Hong Kong–Macao Expressway. The total length of the bridge is 90.3 m, arranged on 3-span with single span length of 30.1 m. The main features of the bridge are given in Table 1. The elevation layout of the bridge and details of the typical cross section are given in Figs. 2 and 3, respectively.

In order to resolve the durability problem of the deck joints, the deck-extension abutments were used. The elevation and plan layouts of the deck-extension abutment are shown in Fig. 4.

The height of the backwalls in the existing drawing was reduced approximately 27 cm to let the approach slabs extend from the end of the superstructures longitudinally across the top of the shortened backwalls. The construction joints were set between the backwalls and the stems to prevent the cracks that are usually produced by the lateral forces on the backwalls due to the friction on the interfaces of the approach slabs and backwalls.

Table 1 – Main features of the Nansanlu Bridge.

Nansanlu Bridge	Feature
Cross section of girder	7 small box girders
Deck width	20.5 m
Beam height	1.6 m
Pavement	120 mm C50 concrete deck + waterproofing layer + 100 mm asphalt deck pavement
Pier type	Column piers: 3 columns with a diameter of 1.5 m
Abutment type	Column abutments: 3 columns with a diameter of 1.5 m
Vehicular load	Highway-I level defined in code (JTG D60-2015)
Skew angle	25°
Bearing	Circle sliding high damping rubber bearing (HDR-D325-H/8) with the design longitudinal movement capacity of 100 mm

One approach slab with a length of 3 m and one transition slab with a length of 3 m were cast at one end of the deck-extension bridge. Two expansion joints with a width of 20 mm were arranged in the approach slab-transition slab connection and the transition slab-connecting road connection, respectively. Therefore, the total longitudinal movement at one end of the superstructure in the deck-extension bridge can reach 40 mm. To reduce the friction on the interface of the approach slab or the transition slab and other components, the sliding material layers were used. The asphalt felts with a thickness of 20 mm were positioned at the top surfaces of the backwalls and sleeper beams. The sand layers with a thickness of 20 mm were arranged at the top surfaces of 150 mm of plain concrete. The foam with a thickness of 50 mm was installed between the side surfaces of the approach slabs/transition slabs and the wing walls of abutments.

The reinforcements were positioned at the mid-depth of the deck to connect the superstructure and the approach slab longitudinally with a horizontal interval of 30 cm to transfer the longitudinal movement of the superstructure to the approach slab. The construction joints were set at the superstructure-approach slab connections. The combination of the longitudinal reinforcements and construction joints can be considered the hinge joints. One softwood strip was installed at the top of each construction joint in the superstructure-approach slab connection to allow a small rotation. To prevent the reflective cracks on the pavement, the reinforced plastic geogrids were arranged at the top of the superstructure-approach slab connections, approach slab-transition slab connections and transition slab-connecting road connections. The asphalt mastics with a width of 30 cm were installed at the approach slab-transition slab connections and transition slab-connecting road connections to prevent the crack in the asphalt pavement when the deck-extension bridge moved longitudinally.

The 250 mm cement-stabilized macadam, 100 mm C15 plain concrete and the sleeper beams with a thickness of 30 cm were arranged under the approach slabs and transition

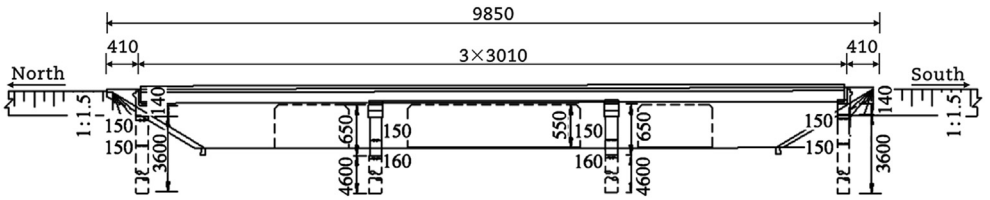

Fig. 2 – Elevation layout of bridge (unit: cm).

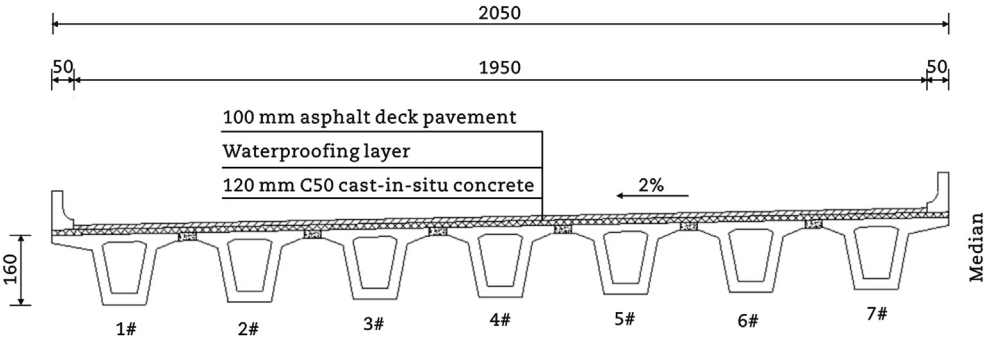

Fig. 3 – Details of the typical cross section (unit: cm).

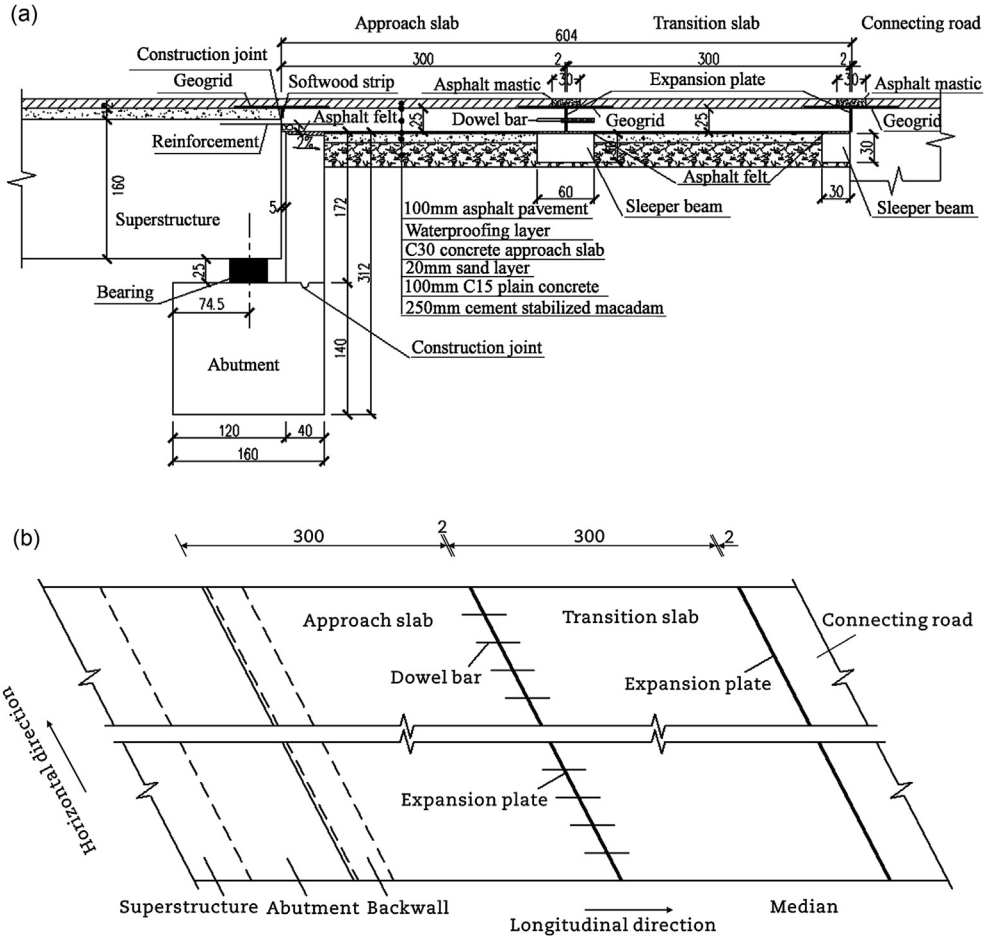

Fig. 4 – Schematic diagram of deck-extension abutment (unit: cm). (a) Elevation layout. (b) Plan layout.

slabs to prevent the settlement. The dowel bars were installed between the approach slabs and the transition slabs to avoid the differential settlements. If there is a theory or calculation in this part, the theory section should extend, not repeat, the background to the article already dealt with in the Introduction, and lay the foundation for further work. In contrast, a calculation section represents a practical development from a theoretical basis.

3. Construction phase

The construction of the deck-extension abutment went through the following phases:

(1) The longitudinal reinforcements were positioned near the end of the superstructure and at the mid-depth of the deck before casting the concrete of the superstructure. The length of the reinforcements in and out of the superstructure should meet the anchorage requirements (Fig. 5(a)). Longitudinal reinforcements can be post-installed for a prefabricated superstructure.

(2) After the compaction of backfill, the 250 mm cement-stabilized macadam, 100 mm C15 plain concrete and the sleeper beams with a thickness of 30 cm were constructed (Fig. 5(a)).

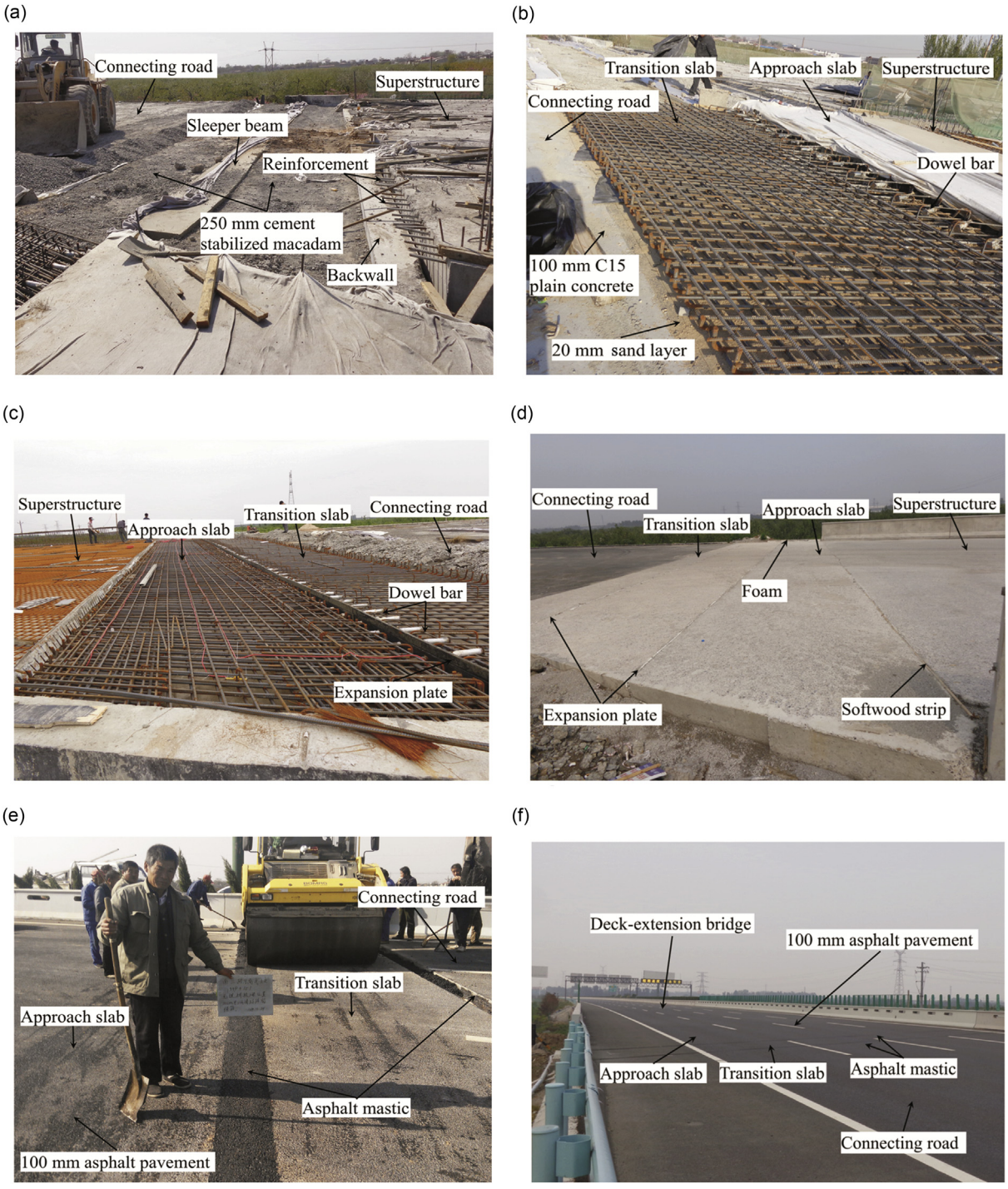

Fig. 5 – Construction phases of deck-extension bridge. (a) Sleeper beam construction. (b) Sand layer arrangement. (c) Reinforcement arrangement. (d) After concrete cast. (e) Pavement construction. (f) Complete deck-extension bridge.

(3) The asphalt felts with a thickness of 20 mm were positioned at the top surfaces of the backwalls and sleeper beams. The sand layers with a thickness of 20 mm were arranged at the top surfaces of the 150 mm plain concrete (Fig. 5(b)). The foam with a thickness of 50 mm was installed between the side surfaces of the approach slabs/transition slabs and the wing walls of the abutments (Fig. 5(d)).
(4) The reinforcements of the approach slabs and the transition slabs were positioned (Fig. 5(c)). The expansion joints with a width of 20 mm and the dowel bars were installed in the approach slab-transition slab connection, and the expansion joints with a width of 20 mm were arranged in the transition slab-connecting road connection (Fig. 5(c)). The softwood strips were installed at the top of the construction joints in the superstructure-approach slab connections (Fig. 5(d)).
(5) The concrete of the approach slabs and the transition slabs was cast (Fig. 5(d)).
(6) The reinforced plastic geogrids and the asphalt mastics with a width of 30 cm were arranged (Fig. 5(e)). The 100 mm asphalt concrete pavements were constructed (Fig. 5(e)).

A final view of the deck-extension bridge is presented in Fig. 5(f).

4. Field test

4.1. Test plan

The overall objectives of this field test were as follows: measurement of the meteorological data on site, temperature distribution on the cross section of the small box girder, longitudinal movement at the end of the superstructure, rotation of the superstructure and the backwall, soil pressure on the backwall and the longitudinal strain of approach slab. The test periods were July 24, 2014–August 4, 2014 and January 20, 2015–January 22, 2015. The meteorological data were measured by a movable automatic meteorological station. Temperature, displacement, soil pressure and strain gauges were installed on the Nansanlu Bridge, as illustrated in Fig. 6.

The temperature gauges installed in the small box girders are shown in Fig. 6(a), including four gauges in the top plate of the girders #1, #3, #5 and #7 (1-T, 3-T, 5-T and 7-T), twelve gauges in the west and east web plates of girders #1, #4 and #7 (1-W1, 1-W2, 1-E1, 1-E2, 4-W1, 4-W2, 4-E1, 4-E2, 7-W1, 7-W2, 7-E1 and 7-E2), three gauges in the bottom plates of girders #1, #4 and #7 (1-B, 4-B and 7-B). Four displacement gauges were installed between the top surfaces of the stems and the bottom surfaces of the girders #1 and #7 at both bridge ends, which can measure the absolute longitudinal movement of the superstructure of the deck-extension bridge because the stems can be considered the fixed point, as illustrated in Fig. 6(b). Four displacement gauges were installed at the superstructure-approach slab connections at both bridge ends to measure the relative longitudinal movement of the superstructure and the approach slabs, as shown in Fig. 6(b) and (c). Four inclinometers were installed on the side surfaces of girders and backwalls at both bridge ends to monitor their rotation angles, as illustrated in Fig. 6(b). Two soil pressure gauges were installed on the back surfaces of backwalls at both bridge ends to measure the earth pressure if the backwalls can move or rotate, as illustrated in Fig. 6(b). Nine concrete strain gauges were embedded in the approach slab to measure the concrete strain, as shown in Fig. 6(c).

4.2. Test results

4.2.1. Temperature results analysis

The results from temperature gauges on August 4, 2014 and January 22, 2015 are summarized in Fig. 7, in which the hollow point denotes the measured temperatures of different parts of the girders, and the solid line denotes the measured ambient air temperature. August 4, 2014 was a sunny day with the highest ambient air temperature and strong solar radiation, and January 22, 2015 was a cloudy day with the lowest ambient air temperature and weak solar radiation.

The temperature results on August 4, 2014 show that the trends in the variation of the temperature of different parts of the girders are similar. The highest temperatures of the top plates are higher (0–1.6 °C) and presented 2 h later than the ambient air temperature, as shown in Fig. 7(a). The highest temperatures of the web plates are equal to or lower than (0–2.7 °C) and are presented 3 h later than the ambient air temperature, as illustrated in Fig. 7(b). The highest temperatures of the bottom plates are lower (2.0 °C–2.8 °C) and presented 3–4 h later than the ambient air temperature, as shown in Fig. 7(c).

The temperature results on January 22, 2015, as illustrated in Fig. 7(d), show that the lowest temperatures of the top plates are higher (4.7 °C–6.7 °C) than and presented approximately 5 h later than the ambient air temperature. The lowest temperatures of the web plates are higher (3.5 °C–6.7 °C) than and presented approximately 2–3 h later than the of ambient air temperature. The lowest temperatures of the bottom plates are higher (4.2 °C–5.3 °C) than and presented 1–2 h later than the ambient air temperature.

4.2.2. Movement results analysis

The small box girders of the Nansanlu Bridge were prefabricated 11 months before the construction. Moreover, the environment-dependent creep and shrinkage of concrete contributes to the partial relief of thermal stresses. However, this relief is relatively small and can be ignored in the design (Oesterle et al., 1999). Therefore, the influences of the shrinkage and creep of concrete on the longitudinal movement were ignored in the research, and the results of the displacement gauges can be considered the longitudinal movement due to temperature variation. The results of the displacement gauges installed at the south end of the bridge from July 24, 2014 to August 4, 2014 are summarized in Fig. 8, in which the hollow point denotes the absolute movement of girders, and the solid point denotes the relative movements between the girders and approach slabs,

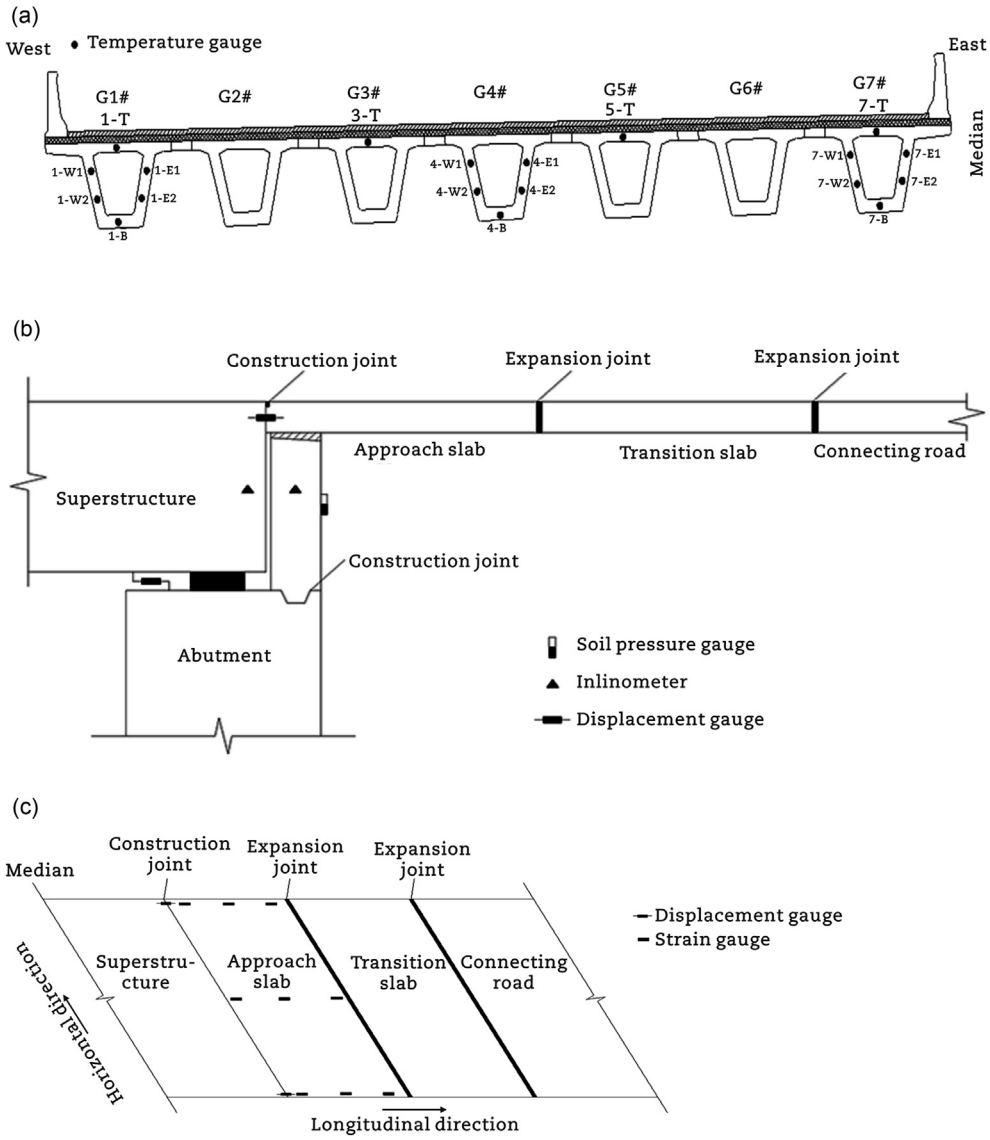

Fig. 6 – Arrangement of measuring points for field test in deck-extension bridge. (a) Cross section of girder. (b) Elevation layout of deck-extension abutment. (c) Plan layout of deck-extension abutment.

because the movement results at both bridge ends were nearly the same. The relative movements between the corresponding girders and approach slabs (−0.02 to 0.32 mm) are significantly smaller than the absolute movements of girders #1 and #7 (−1.64 to 2.15 mm), which are negligible. Therefore, the longitudinal reinforcements connecting the superstructure and the approach slabs can transfer the movements well. From August 4, 2014 to January 22, 2015, the average absolute movement at one end of the superstructure of the Nansanlu Bridge was approximately 15 mm.

4.2.3. *Other test results*

During the monitoring period, the rotation angles of girders and backwalls measured by the inclinometers and the soil pressure on the back surfaces of backwalls measured by the soil pressure gauges at both bridge ends are nearly zero. Therefore, the girders did not rotate, and the backwalls of abutments did not move longitudinally and rotate due to thermal variation. The circle high damping rubber bearing (HDR-D325-H/8) was chosen as the bearings on the abutment, therefore, the friction between the bearings and superstructure can be neglected. Moreover, the sliding materials can effectively reduce the friction on the interface of the approach slab or transition slab and backwalls, wingwalls, 100 mm C15 plain concrete or the sleeper beams. The concrete strain of the approach slab measured by the embedded concrete strain gauges is very small (−0.9 to 10.6 με), which can be neglected. Therefore, the approach slabs can be considered a rigid body during longitudinal movement. Moreover, during the monitoring period, there is no appreciable settlement on the approach slab and the transition slab, and there is also no crack on the pavement, especially at the locations of the superstructure-approach slab connections, approach slab-transition slab connections and transition slab-connecting road connections.

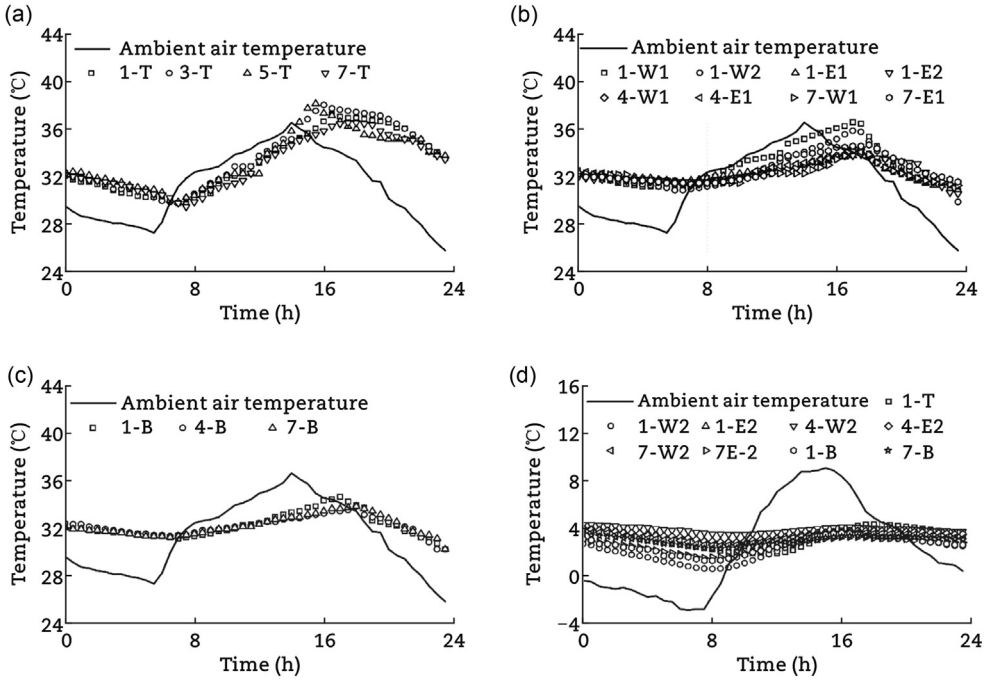

Fig. 7 – Temperature–time curves of different parts of small box girders. (a) Temperature of top plates on August 4, 2014. (b) Temperature of web plates on August 4, 2014. (c) Temperature of bottom plates on August 4, 2014. (d) Temperature of girders on January 22, 2015.

5. Finite element analysis

5.1. *Finite element model*

The 2D plane strain element in the MIDAS program that is suitable for the steady-state or transient heat-conduction analyses was chosen to establish the finite element model (FEM) of the cross section of the small box girder based on the dimensions in Fig. 3, because 2D models are widely used in literature and considered reliable (Elbadry and Ghali, 1983; Lee, 2012; Wang and Fang, 2009). The thermal parameters of the concrete and asphalt used in the finite element model are listed in Table 2 (You, 2011).

The boundary condition of the finite element model was considered by using the measured ambient temperature and solar radiation obtained by the movable automatic meteorological station. The effects of the solar radiation, convective heat transfer and radiative heat transfer at the external surfaces of the small box girder were considered by inputting the surface heat transfer coefficient and the temperature of the surrounding fluid medium as the boundary conditions in the finite element model. The influences of the solar radiation on different parts of the small box girder were considered by using the following rules. The external surface of the top plate is influenced by the beam solar radiation and diffuse solar radiation. The underside of the flange plate and the bottom plate are influenced by the ground reflection. The web plates

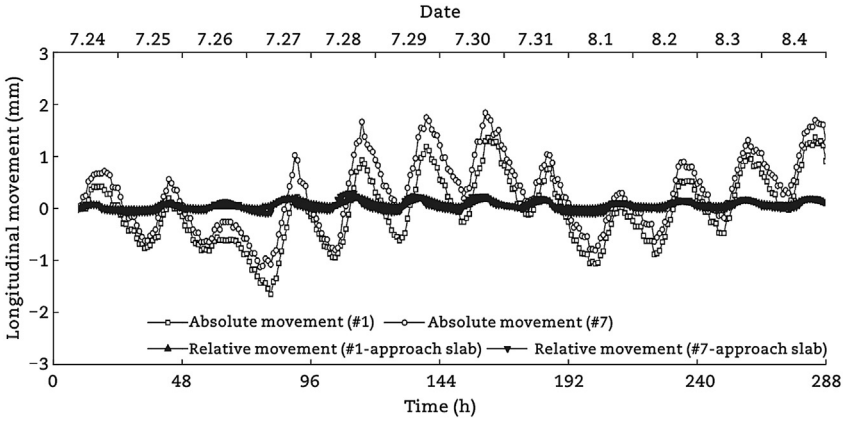

Fig. 8 – Movement-time curves from July 24, 2014 to August 4, 2014.

Table 2 – Thermal parameters of materials used in the finite element model.

Material	Specific heat (J/(kg·°C))	Heat conductivity (W/(m·°C))	Density (kg/m^3)
C50 concrete	920.0	1.740	2500.000
Asphalt	960.0	1.210	2100.000
Air (0 °C)	714.8	0.023	1.293
Air (100 °C)	716.9	0.030	0.946

in the shadow zone are influenced by the combination of the diffuse solar radiation and ground reflection. The web plates that are not in the shadow zone are influenced by the combination of the beam solar radiation, diffuse solar radiation and ground reflection. There is no temperature gauge in the inner space of the small box girder. Therefore, the boundary condition of the internal surface of the small box girder in the finite element model was simulated by using the 2D plane strain element with the thermal parameters of the air (0 °C and 100 °C), as listed in Table 2 (Zhang, 2011). The influence of temperature on the thermal parameters of the air is small. Therefore, the thermal parameters of the air (100 °C) were input in the finite element models subjected to high temperature, and the thermal parameters of the air (0 °C) were input in the finite element models subjected to low temperature.

The number of nodes and elements of the finite element model are 45,632 and 44,786, respectively. The dimension of the mesh is set as 0.02 m, and each node has one degree of freedom of temperature, as illustrated in Fig. 9.

5.2. *Verification of finite element model*

The measured temperature–time curves obtained from temperature gauges and the corresponding calculated temperature–time curves obtained from finite element models on August 4, 2014 and January 22, 2015 are compared in Fig. 10(a) and (b), respectively, in which the hollow point denotes the measured temperature–time curves, and the solid line denotes the calculated temperature–time curves. The trends of both measured and calculated temperature–time curves are nearly the same, and the differences in the ultimate temperatures of both measured and calculated temperature–time curves are less than 1.2 °C on August 4, 2014 and 1.4 °C on January 22, 2015. Therefore, the finite element model described in Section 5.1 can be used to accurately simulate the temperature distribution on the cross sections of the small box girders.

5.3. *Average temperature analysis*

Based on the verified finite element model, the average temperature of the cross section of the small box girder are shown in Fig. 11, in which the hollow point denotes the average temperatures of the cross sections of the small box girders, and the solid line denotes the measured ambient air temperature. The average temperature can be predicted by using the following rules: the total area of the cross sections of the girders was divided by elements. Then, the temperature of each element was calculated by multiplying

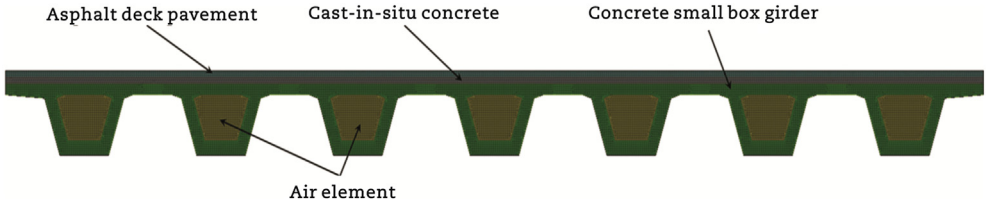

Fig. 9 – Finite element model of cross section of small box girder.

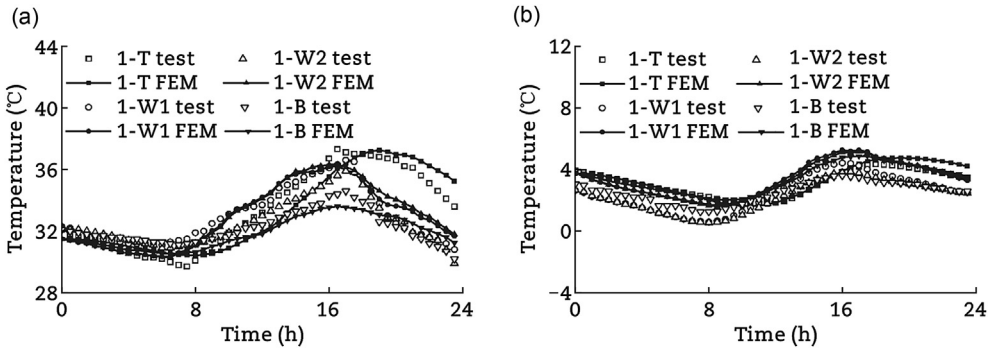

Fig. 10 – Comparison between measured and calculated temperature–time curves of small box girder. (a) August 4, 2014. (b) January 22, 2015.

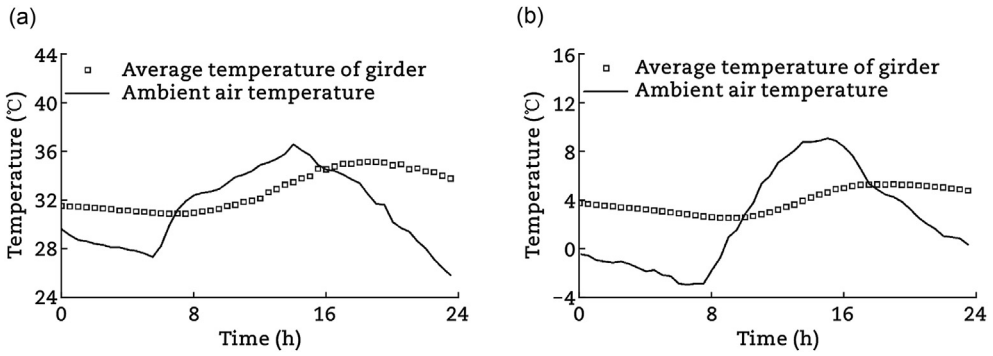

Fig. 11 – Comparison of average temperature of small box girder and corresponding ambient air temperature. (a) August 4, 2014. (b) January 22, 2015.

its area by the corresponding temperature. Finally, the average temperature of the girders can be obtained by dividing the sum of the temperatures of all elements by the total area of the cross sections of girders (Oesterle et al., 1999; Rodriguez et al., 2014). The variation range of the average temperature of the cross sections of the small box girders on August 4, 2014 (4.3 °C) is smaller than the variation range of the ambient air temperature (9.3 °C). The highest value of the average temperature of the cross sections of the small box girders (35.2 °C) is slightly lower (1.4 °C) and presented 4.5 h later than the ambient air temperature (36.6 °C), as shown in Fig. 11(a). The variation range of the average temperature of the cross sections of the small box girders on January 22, 2015 (2.8 °C) is also smaller than the variation range of the ambient air temperature (12 °C). The lowest value of the average temperature of the cross sections of the small box girders (2.6 °C) is significantly higher (5.5 °C) and presented 2.5 h later than the ambient air temperature (−2.9 °C), as shown in Fig. 11(b).

By using Eq. (1), the value of the thermal expansion coefficient of the material (α_c) was chosen as 0.00001 proposed by the code JTG D60-2015 (CCCC Highway Consultants Co., Ltd., 2015), and the temperature calculation length (l_t) was set as 45.15 m, half of the total length of the bridge (90.3 m). Two types of the effective temperature variation (Δt) considered. Type 1: the variation of the average temperatures of the cross sections of small box girders obtained in Section 4.2.1, which is 32.6 °C (the highest value is 35.2 °C and the lowest value is 2.6 °C). The longitudinal thermal movement (Δl) at one end of the superstructure can be calculated as 14.7 mm, which agrees well with the measured movement (15 mm). Type 2: the variation of the characteristic values of effective temperature for the highway bridge structures proposed by the code JTG D60-2015 (CCCC Highway Consultants Co., Ltd., 2015), which is 44 °C for Hebei Province (the highest value is 34 °C and the lowest value is −10 °C). The longitudinal thermal movement (Δl) of the superstructure can be calculated as 19.9 mm, which is 32.7% larger than the measured movement (15 mm). The comparison indicates that the variation of the average temperatures of the cross sections of girders can be used as the effective temperature variation to predict the longitudinal thermal movement of the superstructure in deck-extension bridges with a small box girder.

6. Prediction of maximum longitudinal thermal movement

To predict the maximum longitudinal thermal movement of the Nansanlu Bridge, the extreme conditions of the temperature–time curves, solar radiation–time curves and wind speed should be considered. The 100-year return period was taken into account in this research because the design reference period of a highway bridge is set as 100 years in the code JTG D60-2015 (CCCC Highway Consultants Co., Ltd., 2015). Based on the extreme temperature data of Handan, Hebei Province (1955–2011) obtained from the National Meteorological Information Center, China Meteorological Administration (National Meteorological Information Center, 2018), the yearly highest temperature (43.1 °C) and lowest temperature (−21.3 °C) of Handan, Hebei Province, for the 100-year return period can be predicted by using the normal distribution analysis (Brooks and Carruthers, 1953). The goodness-of-fit of the normal distribution analysis was checked by using the Kolmogorov test (Massey, 1951). The sinusoid model was selected to simulate the daily temperature–time curves. The monthly average daily temperature range of Handan, Hebei Province from 1981 to 2010 can be obtained from the meteorological data centre of the China Meteorological Administration, both 8.9 °C in July and January. The highest temperature of the daily temperature–time curve in July is the yearly highest temperature (43.1 °C), and the corresponding lowest temperature of the curve (34.2 °C) is calculated by subtracting the monthly average daily temperature range in July (8.9 °C) from the yearly highest temperature. Similarly, the lowest temperature of the daily temperature–time curve in January is the yearly lowest temperature (−21.3 °C), and the corresponding highest temperature of the curve (−12.4 °C) is calculated by adding the monthly average daily temperature range in January (8.9 °C) to the yearly lowest temperature. The times at which the ultimate temperatures in the daily temperature–time curves in July and January presented is set as the same as the times in the measured

ambient air temperature curves illustrated in Fig. 7, which are 14:00 for the highest temperature in the daily temperature–time curves in July and 06:00 for the lowest temperature in the daily temperature–time curves in January, respectively. From the news, the extreme temperature in Hebei Province usually continues for approximately four days. The extreme conditions of the temperature–time curves in July and January were denoted by the solid line in Fig. 12.

The extreme conditions of the hourly global solar radiation and the corresponding hourly beam solar radiation of Handan, Hebei Province, in July and January can be simulated by using numerical models (Xue et al., 2018). The wind speed of Handan, Hebei Province, from 1981 to 2010 can be obtained from the meteorological data centre of the China Meteorological Administration, which is 2.4 m/s in July and 2.1 m/s in January.

Based on the verified finite element model in Section 5 and the extreme conditions of the temperature–time curves, solar radiation–time curves and wind speed in July and January mentioned above, the average temperature of the cross sections of the Nansanlu Bridge can be calculated, as denoted by the hollow point in Fig. 12. The variation range of the average temperature of the cross sections of small box girders in the highest temperature condition (3.7 °C) is smaller than the variation range of the ambient air temperature (8.9 °C). The highest value of the average temperature of the cross sections of the small box girders (44.5 °C) is slightly higher (1.4 °C) and presented 4 h later than the ambient air temperature (43.1 °C), as shown in Fig. 12(a). The variation range of the average temperature of the cross sections of the small box girders under the lowest temperature condition (1.7 °C) is also smaller than the variation range of the ambient air temperature (8.9 °C). The lowest value of the average temperature of the cross sections of the small box girders (−17.6 °C) is higher (3.7 °C) and presented 5 h later than the ambient air temperature (−21.3 °C), as shown in Fig. 12(b). By using the variation of the average temperatures of the cross sections of the small box girders (62.1 °C), the maximum longitudinal thermal movement (Δl) of one end of the superstructure of the deck-extension bridge subjected to extreme conditions of temperature, solar radiation and wind speed can be predicted, which is 28.0 mm for Nansanlu Bridge.

7. Conclusions

The following conclusions can be drawn within the limitations of the research presented in this paper.

(1) The design of the deck-extension abutment was introduced in detail to explain the mechanism of transferring the longitudinal movement of the superstructure to the approach slab, which can be used for the most common typology for Chinese continuous beam bridges with small box girders.
(2) The practicability of the jointless design was proved by the construction. Some key technologies, such as the position of longitudinal reinforcements in the superstructure-approach slab connections and the arrangement of the sliding material layers, were introduced.
(3) By comparing the absolute longitudinal movement of girders and the relative longitudinal movements between the girders and approach slabs due to temperature variation, we can prove that the longitudinal reinforcements connecting the superstructure and the approach slabs can transfer the movements well, because the relative longitudinal movements between the girders and approach slabs are very small and negligible.
(4) The girders did not rotate and the backwalls of abutments did not longitudinally move and rotate due to thermal variation, and the sliding materials can effectively reduce the friction on the interfaces, because the rotation angles of girders and backwalls and the soil pressure on the back surfaces of backwalls are nearly zero. The approach slabs moved as a rigid body because the concrete strain of the approach slab is very small and negligible. During the monitoring period, there is no appreciable settlement on the approach slab and the transition slab, and there is also no crack on the pavement.
(5) By comparing the variation of the average temperatures of the cross sections of small box girders, the calculated longitudinal thermal movement at one end of the superstructure agrees well with the measured movement. However, by using the variation of the characteristic

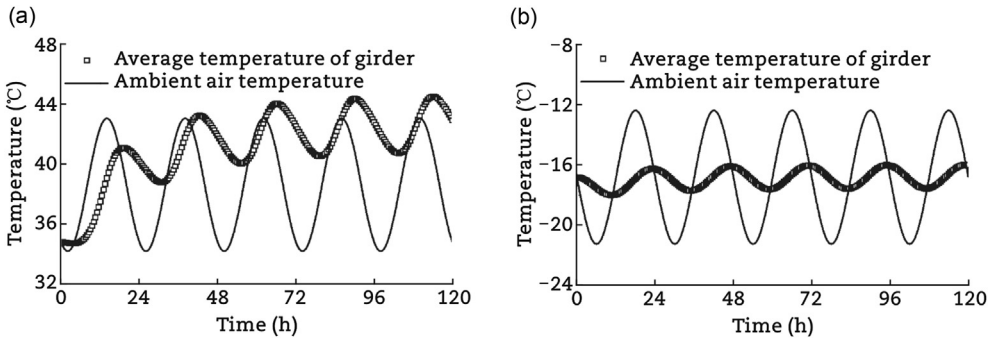

Fig. 12 – Comparison of extreme average temperature of small box girder and corresponding ambient air temperature. (a) Highest temperature condition in July. (b) Lowest temperature condition in January.

values of effective temperature for highway bridge structures proposed by the code JTG D60-2015, the calculated longitudinal thermal movement of the superstructure is 32.7% larger than the measured movement. Therefore, the variation of the average temperatures of the cross sections of the girders can be used as the effective temperature variation to predict the longitudinal thermal movement of the superstructure in deck-extension bridges with the small box girder.

(6) The maximum longitudinal thermal movement of one end of the superstructure of the deck-extension bridge in Hebei Province can be predicted by using the variation of the average temperatures of the cross sections of the small box girders subjected to extreme conditions of temperature, solar radiation and wind speed.

Conflict of interest

The authors do not have any conflict of interest with other entities or researchers.

Acknowledgments

The research was supported by National Natural Science Foundation of China (grant numbers 51508103, 51778148, 51578161), and Recruitment Program of Global Experts Foundation (grant number TM2012-27). The authors would also like to acknowledge the Sustainable and Innovative Bridge Engineering Research Center (SIBERC) of the College of Civil Engineering, Fuzhou University (Fuzhou, China), Hebei Provincial Expressway Shi-an Expressway Extension Project (Hebei, China) and National Meteorological Information Center, China Meteorological Administration.

REFERENCES

Aktan, H., Attanayake, U., Ulku, E., 2008. Combining Link Slab, Deck Sliding Over Backwall, and Revising Bearings. Western Michigan University, Kalamazoo.

Alampalli, S., Yannotti, A.P., 1998. In-service performance of integral bridges and jointless decks. Transportation Research Record 1624, 1–7.

American Association of State Highway and Transportation Officials (AASHTO), 2010. AASHTO LRFD Bridge Design Specifications. American Association of State Highway and Transportation Officials, Washington DC.

Briseghella, B., Zordan, T., 2007. Integral abutment bridge concept applied to the rehabilitation of a simply supported prestressed conventional concrete superstructure. Structural Concrete 8 (1), 25–33.

Briseghella, B., Zordan, T., 2015. An innovative steel-concrete joint for integral abutment bridges. Journal of Traffic and Transportation Engineering (English Edition) 2 (4), 209–222.

Brooks, C.E.P., Carruthers, N., 1953. Handbook of Statistical Methods in Meteorology. Her Majesty's Stationery Office, London.

CCCC Highway Consultants Co., Ltd., 2015. General Specifications for Design of Highway Bridges and Culverts (JTG D60-2015). China Communications Press, Beijing.

Chen, B.C., Zhuang, Y.Z., Briseghella, B., 2014. Jointless Bridge. China Communications Press, Beijing.

Dong, J.C., Xu, Z., Briseghella, B., et al., 2015. Jointless design and construction of existing multi-span simply-supported hollow slab bridge. Journal of China & Foreign Highway 35 (4), 170–174.

Editorial Department of China Journal of Highway and Transport, 2014. Review on China's bridge engineering research: 2014. China Journal of Highway and Transport 27 (5), 1–96.

Elbadry, M.M., Ghali, A., 1983. Temperature variations in concrete bridges. Journal of Structural Engineering 109 (10), 2355–2374.

Fuzhou University, Fujian Provinces No. 1 Highway Engineering Company, 2017. Technical Specifications for Municipal Jointless Bridges in Fujian Province (DBJ/T13-265-2017). Housing and Urban-rural Development of Fujian, Fuzhou.

Husain, I., 2004. Retrofitting of Existing Bridges with Joints to Semi-integral Bridges. Structures Office, Ontario Ministry of Transportation, Ontario.

Jin, X., Shao, X., 2009. A study of fully jointless bridge-approach system with semi-integral abutment. China Civil Engineering Journal 42 (9), 68–73.

Kim, W.S., Laman, J.A., 2010. Numerical analysis method for long-term behavior of integral abutment bridges. Engineering Structures 32 (8), 2247–2257.

Kim, W.S., Laman, J.A., 2012. Seven-year field monitoring of four integral abutment bridges. Journal of Performance of Constructed Facilities 26 (1), 54–64.

Kunin, J., Alampalli, S., 2000. Integral abutment bridges: current practice in United States and Canada. Journal of Performance of Constructed Facilities 14 (3), 104–111.

Lan, C., Briseghella, B., Fenu, L., et al., 2017. The optimal shapes of piles in integral abutment bridges. Journal of Traffic and Transportation Engineering (English Edition) 4 (6), 576–593.

Lee, J.H., 2012. Investigation of extreme environmental conditions and design thermal gradients during construction for prestressed concrete bridge girders. Journal of Bridge Engineering 17 (3), 547–556.

Maruri, R.F., Petro, S.H., 2005. Integral abutments and jointless bridges (IAJB) 2004 survey summary. In: The 2005 FHWA Conference: Integral Abutment and Jointless Bridges, Baltimore, 2005.

Massey, F., 1951. The Kolmogorov – Smirnov test for goodness of fit. Journal of the American Statistical Association 46 (253), 68–78.

Ministry of Transport of the People's Republic of China, 2017. Statistical Bulletin of Development of Transportation Industry in 2016. Ministry of Transport of the People's Republic of China, Beijing.

Munoz, M., Xue, J.Q., Briseghella, B., et al., 2016. Semi static loads in an integral abutment bridge. In: IABSE Conference Guangzhou 2016: Bridges and Structures Sustainability-seeking Intelligent Solutions, Guangzhou, 2016.

National Meteorological Information Center, 2018. Meteorological Data. Available at: http://data.cma.cn/site/index.html (Accessed 28 April 2018).

Oesterle, R.G., Tabatabai, H., Lawson, T.J., et al., 1999. Jointless and Integral Abutment Bridges – Volume III – Summary Report. U.S. Federal Highway Administration, Washington DC.

Rodriguez, L.E., Barr, P.J., Halling, M.W., 2014. Temperature effects on a box-girder integral-abutment bridge. Journal of Performance of Constructed Facilities 28 (3), 583–591.

Shao, X., 2014. New Structures of Jointless Bridge with Semi-integral Abutment. China Communications Press, Beijing.

Wang, J., Fang, Z., 2009. Temperature variation of concrete box girder bridge. Frontiers of Architecture and Civil Engineering in China 3 (4), 407–413.
Weakley, K., 2005. VDOT integral bridge design guidelines. In: The 2005 FHWA Conference: Integral Abutment and Jointless Bridges, Baltimore, 2005.
Xue, J.Q., 2013. Retrofit of Existing Bridges with Concept of Integral Abutment Bridge – Static and Dynamic Parametric Analyses (PhD thesis). University of Trento, Trento.
Xue, J.Q., Briseghella, B., Mazzarolo, E., et al., 2014. Italian national road authority IABs strategy. In: The 7th International Conference on Bridge Maintenance, Safety and Management (IABMAS 2014), Shanghai, 2014.
Xue, J.Q., Briseghella, B., Chen, B.C., et al., 2016. Optimal design of pile foundation in fully integral abutment bridge. Developments in International Bridge Engineering 9, 3–15.
Xue, J.Q., Lin, J.H., Briseghella, B., et al., 2018. Solar radiation parameters for assessing temperature distributions on bridge cross-sections. Applied Sciences 8 (4), 627–654.
You, H.M., 2011. Research on Temperature Distribution Between Box's Interior and Exterior of Prestressed Concrete Box-girder (Master thesis). Fuzhou University, Fuzhou.
Zhang, X.Y., 2011. Practical Handbook of Chemistry. National Defense Industry Press, Beijing.
Zordan, T., Briseghella, B., 2007. Attainment of an integral abutment bridge through the refurbishment of a simply supported structure. Structural Engineering International 17 (3), 228–234.
Zordan, T., Briseghella, B., Lan, C., 2011a. Parametric and pushover analyses on integral abutment bridge. Engineering Structures 33 (2), 502–515.
Zordan, T., Briseghella, B., Lan, C., 2011b. Analytical formulation for limit length of integral abutment bridges. Structural Engineering International 21 (3), 304–310.

Dr. Junqing Xue is an assistant researcher at the College of Civil Engineering, Fuzhou University, China. He received his PhD in civil engineering from University of Trento, Italy, in 2013. His research interests include jointless bridges, retrofit of existing bridges, composite structures.

Dr. Bruno Briseghella is a distinguished professor and dean of the College of Civil Engineering, Fuzhou University, China, and founding director of the "Sustainable and Innovative Engineering Research Center". He graduated with a bachelor's and master's degree from Padova University, Italy, and a PhD from University of Trento, Italy. His main research activities have been focused on bridge and structural design, integral abutment bridges, monitoring and retrofit of bridges, earthquake engineering and composite steel-concrete structures, both from the theoretical and experimental point of view.